ARCHIVES OF ELECTRICAL ENGINEERING VOL. 68(2), pp. 443–454 (2019)

DOI 10.24425/aee.2019.128279

# Modelling and analysis of the low-power 3-phase switched reluctance motor

**MAREK PRZYBYLSKI**

*Tele and Radio Research Institute*
*Ratuszowa 11, 03-450 Warsaw, Poland*
*e-mail: marek.przybylski@itr.org.pl*

(Received: 12.11.2018, revised: 20.03.2019)

**Abstract:** Switched reluctance motors (SRMs) are still under development to maximise their already proven usefulness. A magnetic circuit of the SRM can be made of soft magnetic composites (SMCs). The SMCs are composed of iron powder with dielectric and have a lot of advantages in comparison to commonly used electrical steel. The paper deals with the modelling and analysis of the SRM produced by Emerson Electric Co. for washing machines. Numerical calculations and modelling were done using the FEMM 4.2 program. Magnetic flux densities and magnetic flux lines were calculated, as well as electromagnetic torque and inductance for changing the position of a stator to a rotor. The obtained results were compared with other measurement results and are quite similar. The developed numerical model will be used for the project of a motor with an SMC magnetic circuit.

**Key words:** switched reluctance motor, soft magnetic composites, FEM modelling, dc magnetization curve, iron loss measurement

## 1. Introduction

Drives with switched reluctance motors (SRMs) have a lot of advantages in comparison to other electric drives, such as: comparatively low cost, high rotational speed, simple construction and a lack of permanent magnets. Of course, these drives have some disadvantages such as: high torque ripple, vibration and noise [1, 2]. These drives are of recent interest due to the reduction in the cost of electronic switching elements. Such motors were applied in washing machines named Neptune, manufactured by Maytag Company for the USA market. Both a motor stator and a rotor magnetic core are manufactured with the use of electrical steel sheets. The application of the electrical steel is nowadays frequently replaced with soft magnetic composites (SMCs) made mainly of iron powder and dielectric substance covering each iron particle, ensuring high

resistivity of the material. It ensures low eddy current loss with higher frequencies of magnetic flux. Such composites have a lot of advantages in comparison to electrical steel, such as ease in production magnetic parts with complex shapes. Such a machine's magnetic circuit can be made of a few parts instead of a lot of sheets connected to each other. The mass production of magnetic parts made of powder gives practically no waste of the powder material, whereas during electrical steel punching we have a loss of steel cut from slots and stator edges. It generates additional costs in production of electric motors.

The SRM made by Emerson Electric C., model H55BMBJL-1820 applied in the Maytag washing machines is supplied by a controller supplied from the ac 120 V, 60 Hz line. This drive rated current is $I_{rms} = 2.5$ A. The SRM enables working in a wide speed range and with high low-speed torque. The maximum rotational speed of a rotor for top washing machine spinning is equal to about $n = 11200$ r/min. For this rotational speed, the fundamental frequency of a phase current is equal to $f_1 = (n \cdot N_r)/60 = (11200 \cdot 8)/60 = 1493$ Hz, $N_r$ number of poles in a rotor. The flux waveforms in the SRMs have not only the fundamental frequency, a frequency of $f = m \cdot f_1$ ($m = 3$, the number of phases), but they have also higher harmonic content and flux waveforms are different in different parts of the magnetic circuit [3]. That is why the determination of iron loss in a SRM is very difficult. The high frequency of magnetic flux causes high energy loss in the magnetic circuit of the motor and usage of SMCs should decrease this loss.

The main aim of the research is to design, manufacture and measure the performance of a SRM with the use of SMC material in its construction. A lot of efforts are put into the construction of SRMs with the SMC material core [5–11]. The work will enable one to compare the performance of the developed motor with the SRM produced by Emerson Electric Co. The SR motors could be produced cheaper and with performance comparable to the original one. For this reason, the modelling and analysis of the motor made by Emerson Electric Co. is the first step in the process of redesigning the motor.

## 2. Determination of electromagnetic properties of the switched reluctance motor

It is essential to measure magnetic properties of electrical steel sheets used in a Maytag motor construction for a proper modelling of an SR motor. The next step is to identify the number of turns and configuration of windings. The last thing is to take precise measurements of dimensions of the existing motor.

### 2.1. Determination of magnetic properties of soft magnetic core of the motor

The DC magnetization curve $B = f(H)$ of a stator and rotor material was measured according to the IEC 60404-4 standard on a ring sample, whereas the measurements of iron loss vs magnetic flux density and frequency according to the IEC 60404-6 standard. The outer diameter of the sample is 60.1 mm and the inner diameter is 40.2 mm. The ring sample was composed of 13 sheets cut from the rotor. The thickness of each sheet is 0.7 mm. Both the rotor and stator are made of the same steel sheet. The density of the sample is 7.21 g/cm$^3$. The measurements were taken with the use of a hysteresisgraph made by Laboratorio Elettrofisico, an AMH 20K-HS model.

The sample was wound with two wires. The first winding for determining magnetic flux density had 45 turns with 0.55 mm in diameter, whereas the second one for determining magnetic field strength had 170 turns with 0.75 mm in diameter.

Fig. 1 shows the measuring sample for magnetic properties measurements.

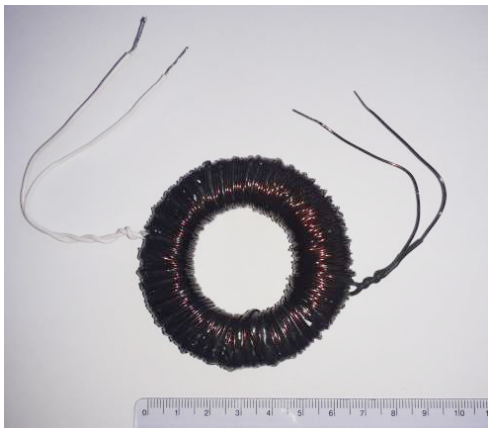

Fig. 1. Measuring sample for magnetic properties

Fig. 2 shows a static magnetization characteristic of the stator and rotor magnetic core. For a low magnetic field strength of up to 1 000 A/m, magnetic flux density increases almost linearly. For higher magnetic field intensity we can observe the saturation process of the magnetic flux density, which reaches 1.56 T for $H$ = 5 800 A/m. The maximum value of magnetic permeability is 1 480 for a magnetic field strength equal to 440 A/m.

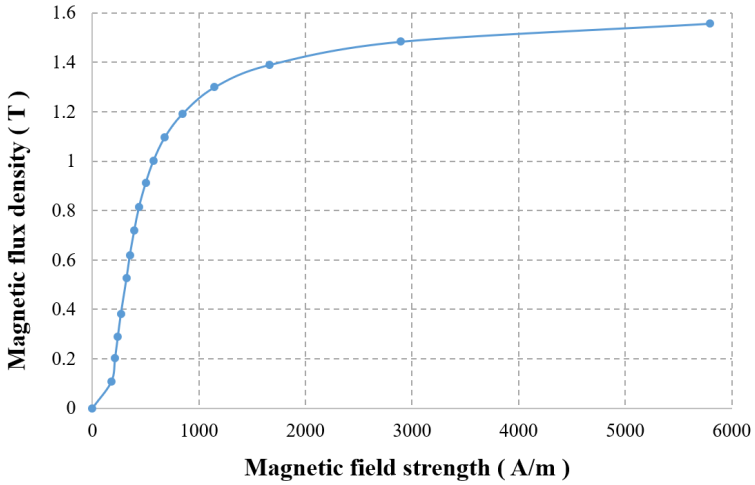


Fig. 2. Static magnetization curve of stator and rotor magnetic core

In the next step of the work, AC measurements of iron loss vs magnetic flux density and its frequency were conducted. The magnetic flux density during the measurements was kept

sinusoidal with a form factor of 1.11 ± 1%. The iron loss was determined from 50 to 2 000 Hz. The results of the measurements are shown in Fig. 3.

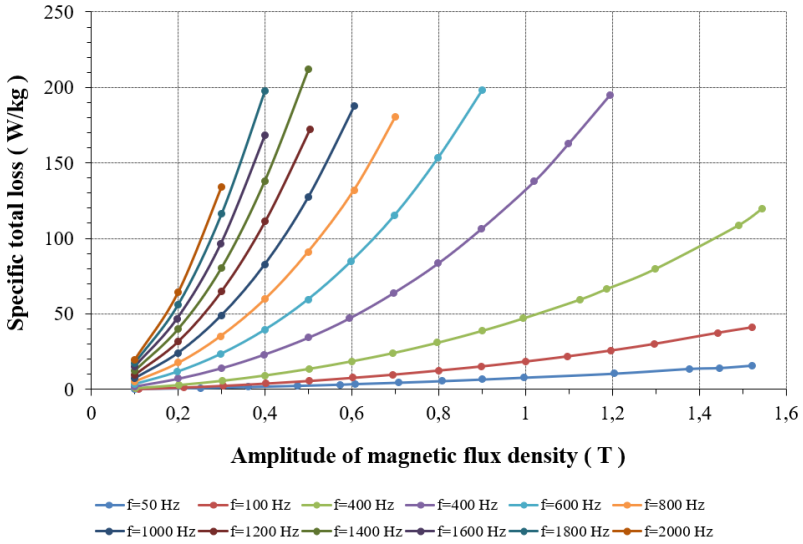


Fig. 3. Iron loss of sample vs magnetic flux density and its frequency

According to the measurements, the iron loss for the sample composed of 0.65 mm sheets cut from the motor is very high in comparison to the iron loss for samples with the same thickness, determined in accordance with the EN standard. According to the EN 10106 standard, the iron loss for M470-65A electrical steel at 50 Hz, for 1 T is $\Delta P_{\mathrm{Fe}} = 2$ W/kg, for 1.5 T $\Delta P_{\mathrm{Fe}} = 4.7$ W/kg, whereas for the steel of the SRM at 50 Hz for 1 T it is $\Delta P_{\mathrm{Fe}} = 7.8$ W/kg, for 1.5 T $\Delta P_{\mathrm{Fe}} = 15.9$ W/kg. The iron loss from the sheets of the SRM in the same conditions is 3.4÷3.9 times higher than from the EN standard samples. This increase of loss is caused not only by the processing of steel sheets into the magnetic core, but also by the difference in the type of sheets. The differences for higher frequencies are very difficult to compare because producers do not show iron loss for frequencies higher than 50 Hz.

### 2.2. Determination of electric parameters of the motor

In order to model a motor it is essential to determine properties of an electric circuit of the motor. Fig. 4(a) shows a structure of the SRM with windings. The motor has 3 phases, 12 stator poles and 8 rotor poles. The configuration of the windings is shown in Fig. 4(b).

The number of turns of each coil is equal to 172. Each coil is wound with a copper wire having a diameter of 0.56 mm.

Table 1 shows parameters of the motor.

Determination of electric and magnetic parameters of the Maytag motor enabled its numerical modelling and simulations.

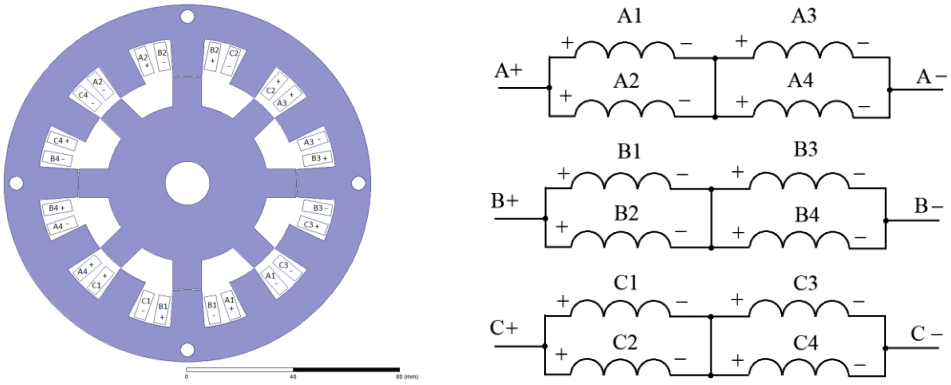


(a) (b)

Fig. 4. Structure of the 3-phase switched reluctance motor (a), configuration of 3-phase windings of the switched reluctance motor (b)

Table 1. Parameters of the Emerson Electric Co. switched reluctance motor

| **Parameter** | **Value** | **Unit** |
|---|---|---|
| DC supply voltage | 170 | V |
| Rated rms current | 2.5 | A |
| Range of rotational speed | 700÷11 200 | r/min |
| Stator outer diameter | 139.5 | mm |
| Stator inner diameter | 83.8 | mm |
| Width of a stator tooth | 11.0÷12.7 | mm |
| Stator magnetic core thickness | 13.1 | mm |
| Stator slot area | ~ 200 | $mm^2$ |
| Rotor outer diameter | 83 | mm |
| Rotor inner diameter | 61 | mm |
| Width of a rotor tooth | 11 | mm |
| Shaft diameter | 17 | mm |
| Thickness of the air gap | 0.4 | mm |
| Axial thickness of a magnetic core | 47.3 | mm |
| Number of phases | 3 | |
| Number of stator poles | 12 | |
| Number of rotor poles | 8 | |
| Number of turns in a coil | 172 | |
| Diameter of a copper wire | 0.56 | mm |
| Copper fill factor in a slot | ~ 0.4 | |

## 3. Numerical modelling of the motor

The FEMM 4.2 software developed by David Meeker was used for numerical modelling of an SRM. This software is based on a finite element method (FEM). The SRM can be modelled in two dimensions, because the motor has a planar symmetry. Fig. 5 shows the model of an SRM created in the mentioned software. Fig. 5 shows also a discretization mesh used in calculations. For obtaining good results of calculations, three layers of triangular elements were modelled in the air gap of the motor. The SRM model is discretized using approximately 100 000 elements with 50 000 nodes.

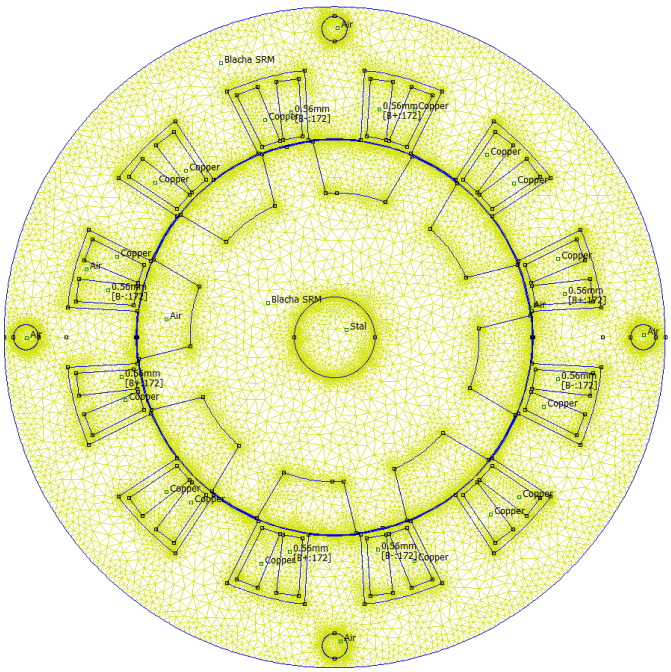


Fig. 5. Switched reluctance motor with discretization mesh modelled in FEMM 4.2 software

The analysis of the motor was conducted for a 1-phase mode. It is assumed that only one phase is supplied with a direct current. When running a real motor for a defined period of time, only one phase is working. Each phase is independent of other phases. Each phase is supplied from a converter with rectangular rectified voltage. It ensures a direct current in a phase that resembles a triangle.

Distribution of static magnetic field in a motor is described by differential Eq. (1):

$$rot\left(\frac{1}{\mu}\, rot\, \boldsymbol{A}\right) = \boldsymbol{J}, \tag{1}$$

where: $\boldsymbol{A}$ is the magnetic vector potential, $\mu$ is the magnetic permeability, $\boldsymbol{J}$ is the electric current density.

Because $\boldsymbol{J}$ has only one component not equal to zero, $J_z \neq 0$, therefore $\boldsymbol{A}$ has only one component not equal to zero, $A_z \neq 0$. Magnetic vector potential $A_z = 0$ was set on an outer region of the motor.

## 4. Numerical analysis of the motor

Magnetic flux densities in the motor and in the air gap for a 2.5 A dc in phase B were calculated for an aligned position of the rotor and the stator as well as an angle of 14° of the rotor position in relation to the stator. At this 14° arrangement between the stator and rotor, the motor develops the maximum value of electromagnetic torque, $T = 0.47\ N{\cdot}\text{m}$ for a 2.5 A current (Fig. 6(a)). Fig. 6(a) shows magnetic flux density in the motor for the aligned position, whereas Fig. 6(b) shows magnetic flux density for the 14° position. The maximum value of the magnetic flux density is about 0.7 T.

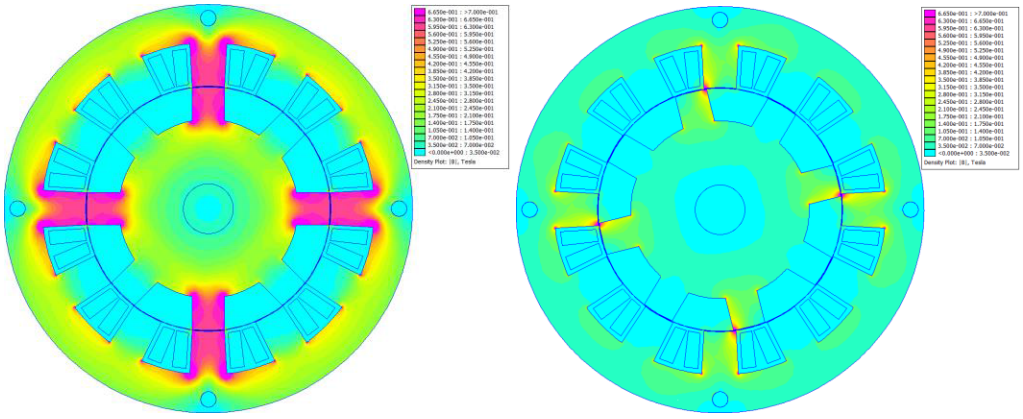

(a) (b)

Fig. 6. Magnetic flux density distribution in the switched reluctance motor: for aligned position of rotor and stator (a) and 14° angle of rotor and stator; $I_B = 2.5$ A, $B_{\max} = 0.7$ T (b)

Fig. 7(a) shows magnetic flux density distribution in the air gap of the motor for the aligned position, whereas Fig. 7(b) shows it for a 14° angle between the rotor and stator. The maximum value of the magnetic flux density in the air gap in the first case is about 0.6 T, whereas in the second case it is about 0.65 T.

Fig. 8(a) shows magnetic flux lines in the motor for the aligned position and Fig. 8(b) for a 14° angle between the rotor and stator.

Electromagnetic torque courses of an Emerson Electric Co. motor were measured with a changing position of the rotor to the stator. Fig. 9 shows a measuring stand for determination of electromagnetic torque developed by an SRM. In order to measure the motor torque, its rotor rotates with a low speed of 0.8 r/min. The difference between the driving motor torque and SRM motor torque supplied by a 2.5 A dc current is measured by a torque meter. The motor was supplied

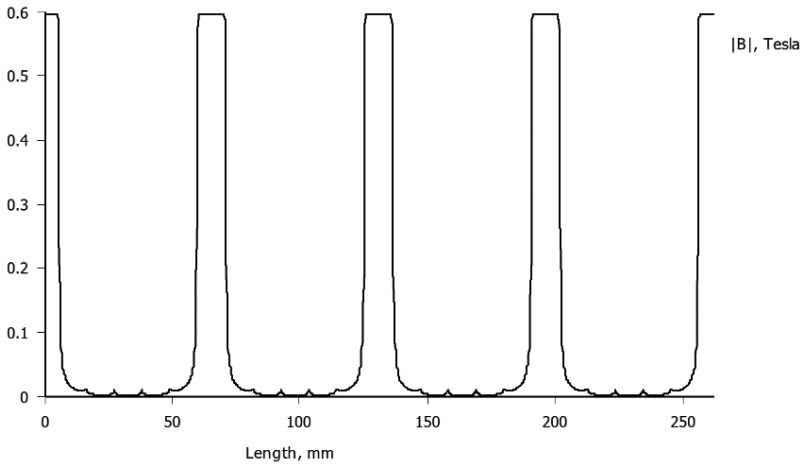


(a)

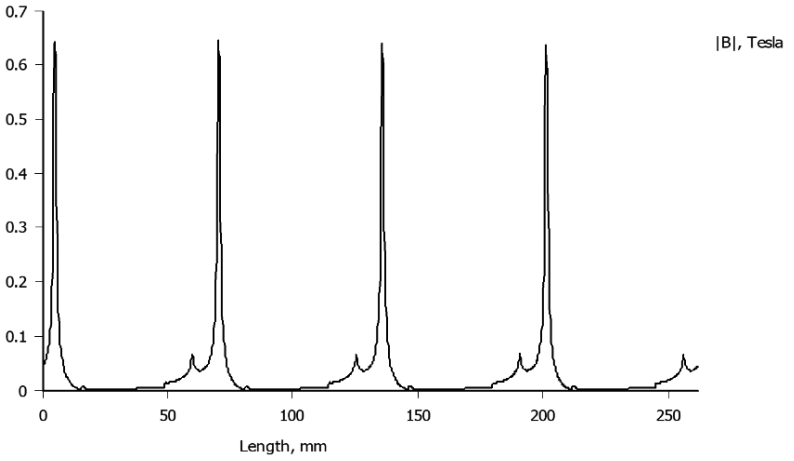


(b)

Fig. 7. Magnetic flux density in the air gap of the motor: for aligned position of rotor and stator $B_{\max} = 0.6$ T (a); 14° angle between rotor and stator $B_{\max} = 0.65$ T, $I_B = 2.5$ A (b)

from GW Instek PSP-2010 power supply, the current was measured by a Fluke 115 multimeter, whereas the motor torque by an MW 2006-3S torque meter with a MT-3Nm sensor made by Pracownia Elektroniki Poznan. The measured course of the torque in Fig. 10(a) is composed of 470 points.

Electromagnetic torque for different rotor positions for a 2.5 A dc in phase B was determined. The torque was calculated using a weighted stress tensor [4]. Fig. 10(a) shows the courses of electromagnetic torque measured and simulated as a function of a rotor and stator position. The calculated electromagnetic torque resembles a rectangle with a maximum value of 0.47 N·m, whereas the measured one – 0.62 N·m.

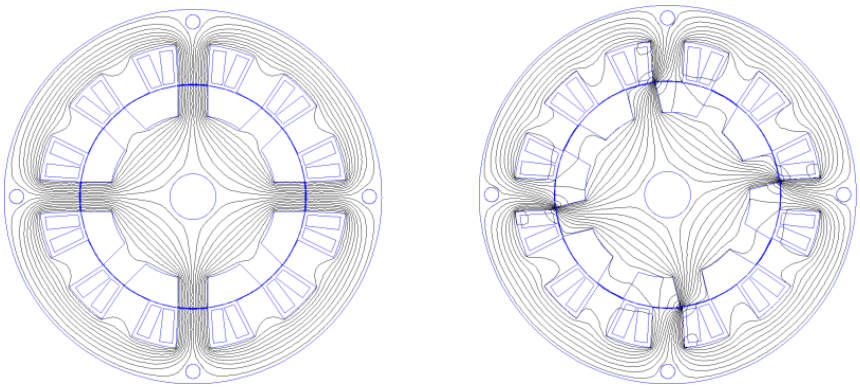

(a) (b)

Fig. 8. Magnetic flux lines in the motor: aligned (a); 14° angle between rotor and stator, $I_B = 2.5$ A (b)

Fig. 9. Measuring stand for determination of SRM torque

The difference between the measurements and calculations is about 24%. This is, among others, caused by 2 dimensional simulations, which are not influenced by end windings and end effects. The electromagnetic torque was also calculated on the basis of inductance measurements. The torque was then calculated based on changes of inductance for an altering rotor position multiplied by 0.25 and the current in the second power. For the same current $I = 2.5$ A, the calculated maximum electromagnetic torque was equal to 0.53 N·m [12]. Here, the difference is equal to 11%.

The course of inductance for different rotor positions was calculated for a 2.5 A dc in the phase B. The inductance calculations were performed using the volume integration of magnetic vector potential and current density product in the windings [4]. Fig. 10(b) shows the inductance course as a function of a rotor position. The course of inductance is triangular and changes from about 6 mH to 48 mH.

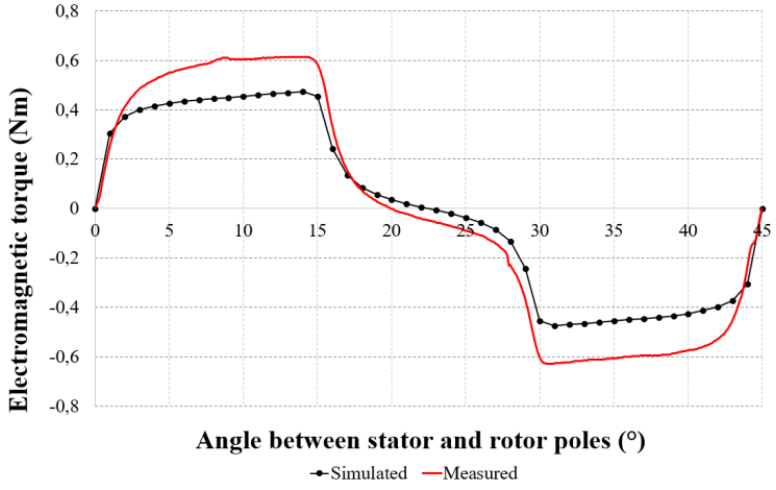


(a)

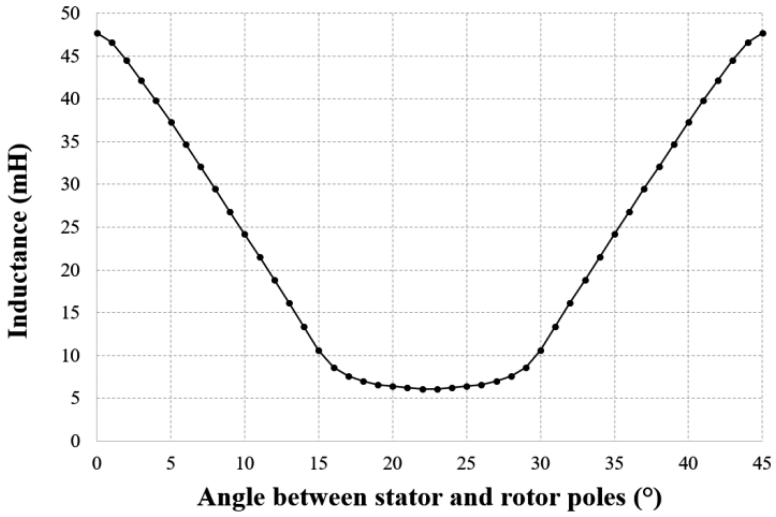


(b)

Fig. 10. Measured and calculated electromagnetic torque vs rotor positions (a), phase B inductance vs rotor position; $I$ = 2.5 A (b)

Flux linkage with phase B was calculated as a function of phase currents. The calculations were done for an aligned and unaligned stator against a rotor position. Fig. 11 shows courses of the flux linkage for the current from 0 to 6 A. The saturation effect can be observed for currents above 5.5 A. For lower currents, the dependence of the flux linkage is almost linear.

The data from Fig. 11 enables one to calculate the average torque $T_{avg}$ from the loop area $W$ bordered by the linkages in an aligned and unaligned positions and the current. Eq. (2) shows the

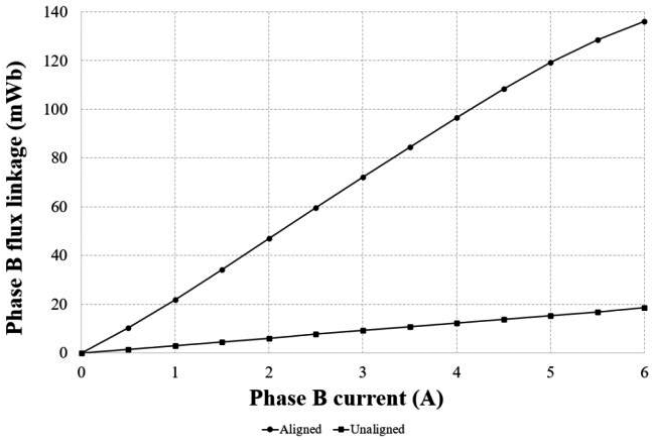


Fig. 11. Phase B flux linkage vs current for aligned and unaligned rotor and stator position

formula to calculate [3]:

$$T_{\text{avg}} = \frac{SW}{2\pi} = \frac{mN_r W}{2\pi}, \tag{2}$$

where: $S$ is the number of strokes per revolution, $m$ is the number of phases $m = 3$, $N_r$ is the number of rotor poles, $W$ defines the energy converted from electrical to mechanical.

For $I = 2.5$ A, the average torque calculated from (2) is equal to 0.25 N·m.

Fig. 12 shows the maximum electromagnetic torque as a function of current in phase B for an angle of 14° between the stator and rotor poles. At a 14° angle, the motor develops the maximum electromagnetic torque. As it can be seen, with the increase of current in the phase, the electromagnetic torque increases quadratically. For $I = 2.5$ A, the maximum electromagnetic torque is equal to 0.47 N·m, as it was mentioned earlier.

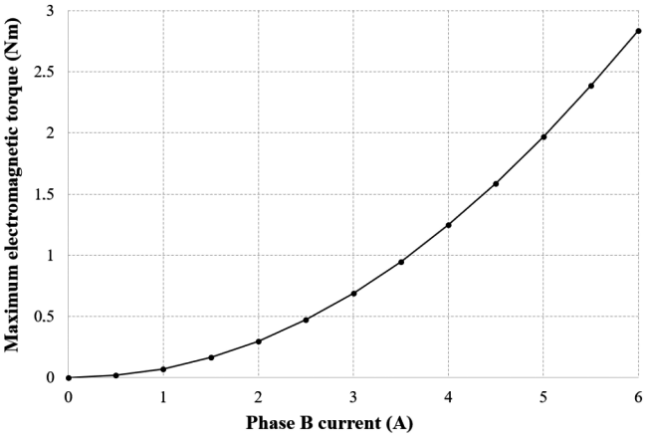


Fig. 12. Maximum electromagnetic torque vs phase B current, 14° angle between rotor and stator positions

## 5. Conclusions

The comparison of the results of modelling with the measurements results shows that the developed computer model is quite good. Differences between calculations and measurements are caused by 2-dimensional modelling, without the influence of the windings outside the grooves on parameters of the motor. The developed computer model will be used for the project of an SRM with a soft magnetic composite magnetic circuit. This will allow comparison of calculations of Emerson Electric Co. motor to a newly developed motor with soft magnetic composite. The model motor will be built in the housing of motor made by Emerson Electric Co.

**References**

[1] Miller T.J.E., *Brushless Permanent-Magnet and Reluctance Motor Drives*, Oxford University Press (1989).

[2] Krishnan R., *Switched reluctance motor drives: Modelling, Simulation, Analysis, Design, and Applications*, CRC Press (2001).

[3] Miller T.J.E., *Optimal design of switched reluctance motors*, IEEE Transactions on Industrial Electronics, vol. 49, no. 1, pp. 15–27 (2002).

[4] Meeker D., *Finite Element Method Magnetics – User's Manual ver. 4.2*, pp. 41–43 (2018).

[5] Gaing Z.L., Kuo K.Y., Hsieh J.S., Tsai M.H., *Design and optimization of high-speed switched reluctance motor using soft magnetic composite material*, International Power Electronics Conference (IPEC), Hiroshima, Japan, pp. 278–282 (2014).

[6] Lenin N.C., *Experimentation of three phase outer rotating switched reluctance motor with soft magnetic composite materials*, Journal of Engineering Science and Technology, vol. 12, pp. 54–61 (2017).

[7] Nikam S.P., Fernandes B.G., *Design of soft magnetic composite based modular four phase SRM for electric vehicle application*, International Conference on Electrical Machines (ICEM), Berlin, Germany, pp. 112–116 (2014).

[8] Karthikeyan R., Vijayakumar K., Arumugam R., *Soft magnetic composite switched reluctance generator – fabrication and analysis*, International Conference on Manufacturing Science and Technology (ICMST), Singapore (2011).

[9] Vijayakumar K., Karthikeyan R., Arumugam R., Premsunder G., Kannan S., *Coupled field finite element analysis of switched reluctance motor with soft magnetic composite material for thermal characterization*, International Conference on Industrial and Information Systems, Peradeniya, Sri Lanka (2009).

[10] Vijayakumar K., Karthikeyan R., Arumugam R., *Influence of soft magnetic composite material on the electromagnetic torque characteristics of switched reluctance motor*, Joint International Conference on Power Systems Technology (POWERCON), New Delhi, India, pp. 1110–1115 (2009).

[11] Vijayakumar K., Karthikeyan R., Sathishkumar G.K., Arumugam R., *Two dimensional magnetic and thermal analysis of high speed switched reluctance motor using soft magnetic composite material*, IEEE Region 10 Conference (TENCON), Hyderabad, India, pp. 1566–1570 (2008).

[12] Di Barba P., Mognaschi M.E., Wiak S., Przybylski M., Ślusarek B., *Optimization and measurements of switched reluctance motors exploiting soft magnetic composite*, International Journal of Applied Electromagnetics and Mechanics, vol. 57, pp. S83–S93 (2018).